AECL-9717

ATOMIC ENERGY OF CANADA LIMITED

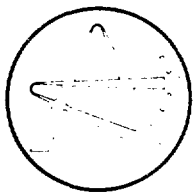

L'ÉNERGIE ATOMIQUE DU CANADA LIMITÉE

AN ISOTOPE SEPARATION MAGNET FOR THE INJECTOR TEST EXPERIMENT (MITE)

AIMANT DE SÉPARATION D'ISOTOPES POUR L'APPAREIL D'ESSAIS D'INJECTEUR (MITE)

T. TAYLOR, T. TRAN NGOC and E.C. DOUGLAS

Chalk River Nuclear Laboratories Laboratoires nucléaires de Chalk River

Chalk River, Ontario

March 1988 mars

ATOMIC ENERGY OF CANADA LIMITED

AN ISOTOPE SEPARATION MAGNET FOR THE INJECTOR TEST EXPERIMENT (MITE)

T. Taylor, T. Tran Ngoc and E.C. Douglas

Accelerator Physics Branch
Chalk River Nuclear Laboratories
Chalk River, Ontario K0J 1J0

1988 March

AECL-9717

L'ÉNERGIE ATOMIQUE DU CANADA, LIMITÉE

AIMANT DE SÉPARATION D'ISOTOPES POUR L'APPAREIL D'ESSAIS D'INJECTEUR (MITE)

par

T. Taylor, T. Tran Ngoc et E.C. Douglas

RÉSUMÉ

On a conçu un aimant pour les études de neutralisation de la charge spatiale avec l'Appareil d'Essais d'Injecteur des Laboratoires Nucléaires de Chalk River. En y ajoutant des collecteurs appropriés, on pourrait également se servir de l'aimant pour les séparations d'isotopes à l'échelle expérimentale. Le présent rapport documente la conception de cet aimant particulier et illustre en général la technique de conception des aimants de transport de faisceaux.

Physique des accélérateurs
Laboratoires Nucléaires de Chalk River
Chalk River, Ontario K0J 1J0
1988 mars

AECL-9717

ATOMIC ENERGY OF CANADA LIMITED

AN ISOTOPE SEPARATION MAGNET FOR THE INJECTOR TEST EXPERIMENT (MITE)

T. Taylor, T. Tran Ngoc and E.C. Douglas

ABSTRACT

A magnet has been designed for space-charge neutralization studies on the Injector Test Experiment at the Chalk River Nuclear Laboratories. Augmented by suitable collectors, the magnet could also be used for pilot-scale isotope separations. The present report documents the design of this particular magnet and illustrates the process of designing beam transport magnets in general.

Accelerator Physics Branch
Chalk River Nuclear Laboratories
Chalk River, Ontario K0J 1J0

1988 March

AECL-9717

Table of Contents

1. INTRODUCTION

The throughput of an electromagnetic isotope separator is determined by two principal factors. The first is the brightness of the ion source and the second is the acceptance of the ion optical system.

The CRNL duoPIGatron ion source[1,2] can generate brighter beams than the ion sources traditionally used for stable isotope separation. This raises the possibility of electromagnetic isotope separators with higher throughput producing stable isotopes more cheaply. However, at the high intensities that are required for the cost effective separation of stable isotopes, the beam transport can be dominated by space-charge[3,4] necessitating ion optical systems with inordinately large acceptance.

Fortuitously, the fast ions that comprise the beam collide with the atoms of the residual gas in the vacuum system generating free electrons. Provided that the beam is stable, the electrons are trapped inside the beam neutralizing the space charge. Of course, the residual gas that is essential for space-charge neutralization also removes ions from the beam by charge exchange. Obviously the efficacy of space-charge neutralization by residual gas is limited.

Neutralization is, in fact, a complex process that is far from understood. It would be imprudent to invest in a full-scale stable isotope production facility without further research. The Injector Test Experiment (ITE) at the Chalk River Nuclear Laboratories with the addition of a suitable isotope separation magnet would be ideal for studies of space-charge neutralization.

An appropriate Magnet for ITE (MITE) has now been designed. Augmented by suitable collectors, the MITE could also be used for pilot-scale isotope separations. The present report documents the MITE design and illustrates the process of designing beam transport magnets in general.

2. SPECIFICATIONS

An isotope separator enhances the concentration of one (or more) of the isotopes of an element with respect to the concentrations of all of the other isotopes of

the element. Thus, the most fundamental parameter in the design of a separation magnet is the enhancement factor, EF, defined by[5]

$$EF = (C_{fw}/C_{fu})/(C_{iw}/C_{iu}) \quad [1]$$

where the concentrations, C, are subscripted f and i to denote final and initial and w and u to indicate the wanted and the unwanted isotopes. The enhancement factor for a given separator is a function of the relative mass difference of the wanted and the unwanted isotopes. The most challenging separation that is of immediate interest here involves the enrichment of tellurium to greater than 99% ^{124}Te, requiring an enhancement factor of at least 170 at a relative mass difference of only 0.8%.

A separation magnet must have a large acceptance so that the intense ion beams that are essential to a high throughput can be transmitted. The ion beam from the CRNL duoPIGatron ion source with a normalized (proton equivalent) current of 600 mA at an extraction voltage of 50 kV has a waist approximately 4 mm by 20 mm with a divergence of about 60 mradians at 2% of the maximum intensity. In addition, a separation magnet must simultaneously transit all of the stable isotopes of a given element. The element with the largest mass range is calcium. Simultaneous transmission of ^{40}Ca and ^{48}Ca requires a minimum momentum acceptance of 9%.

The magnet must be able to bend the most rigid ion that is of interest which, in the present case, is a singly ionized thallium atom with an energy of 50 keV.

The vacuum chamber must be cooled to dissipate the heat generated by beams with normalized currents of 60 mA and energies of 50 keV. The limiting case is helium with an absolute current of 300 mA in a single species. (Although helium is not likely to be separated with the proposed magnet, helium may well be used in ITE for experiments unrelated to isotope separation.)

Finally, the magnet must be small enough to fit into the available space, reliable, easy to service, as simple as is consistent with all of the preceding considerations, and, including the power supply and the vacuum chamber, as inexpensive as is possible.

3. ION OPTICS

3.1 First Approximation

Keeping in mind the need for simplicity and the shape of the available space, a 90° sector magnet with a homogeneous magnetic induction was chosen. Double focusing was achieved by rotating both the entrance face and the exit face through 26.6° and setting both the object distance and the image distance to two times the bending radius. (See Case 7 of Ref. 6.)

The minimum acceptable bending radius is dictated, in the present case, not by the requisite enhancement factors but by the minimum distance between adjacent isotopes that is sufficient to accommodate collectors. The perpendicular distance, d, between the trajectories of masses M and M+δM at the focal plane is given by[5]

$$d = DR_o \delta M/M \qquad [2]$$

where D is the dispersion corresponding to a given separator geometry and R_o is the mean bending radius of the magnet. It can be shown[6] that D=2 for the configuration under consideration here. (Note that Ref. 6 uses absolute momentum dispersion rather than the relative mass dispersion used here and in Ref. 5. Thus the D of Ref. 6 is $2R_o$ times the D of Ref. 5.) If a separation of at least 10 mm is required between isotopes with a mass difference of 0.8% then the minimum acceptable bending radius is 620 mm.

Aberrations associated with the large radial divergence of the beam can be suppressed to second order by radiusing the entrance and exit faces of the magnet. The appropriate radii, R' and R", are given by[6]

$$\frac{1}{R'} + \frac{1}{R''} = \frac{2R_o}{L^2}\left[\frac{R_o}{L} + 3\tan\varepsilon\right]\cos^3\varepsilon \qquad [3]$$

where L is the object (or image) distance and ε is the pole face rotation. Setting R'=R" yields a radius of 1.73 m in the present case.

Choosing a pole gap approximately one and one half times the height of the beam, a minimum gap of 120 mm is dictated by the 77 mm axial extent of the beam following a 1.24 m drift.

Figure 1 shows that the proposed separator can be accommodated in the available space. To confirm that the first approximation design gives a sufficiently large enhancement factor, we assume the peak shape of Ref. 5. Choosing the image slit to transmit 90% of the beam, we calculated an enhancement factor of about 300 for ^{124}Te, almost twice the required value. Furthermore, the 4 mm object width assumed here is somewhat pessimistic. A factor of two reduction in the object width would increase the enhancement factor to approximately 800.

3.2 Computerized Optimization

The separator was modeled with the beam transport code, TRANSOPTR[7], using a second order matrix formalism. In addition to the parameters derived earlier, TRANSOPTR requires field profile coefficients. The values recommended by Brown[8] for square pole edges, namely 0.45 and 2.8 for k_1 and k_2 respectively, were adopted as a first approximation.

It was immediately apparent that the axial focusing provided by the first approximation design was inadequate. The axial extent of the beam at the exit face of the magnet was far greater than at the entrance face. The entrance pole face rotation was increased to 32.7° so that the beam height at the exit face was no greater than the beam height at the entrance face. The exit pole face rotation was reduced to 20.6° to return the radial image to its original position. (This leaves the system slightly astigmatic. Stigmatic focusing could be achieved, although only at the expense of dispersion, by reducing the exit pole face rotation still further. However, an axially defocused beam is actually to be preferred because the power density at the isotope collector is then reduced slightly.) Finally, the radial aberrations were minimized by adjusting the entrance and the exit pole face radii to infinity and 930 mm respectively.

The revised design has very slightly reduced dispersion with marginally improved enhancement factors.

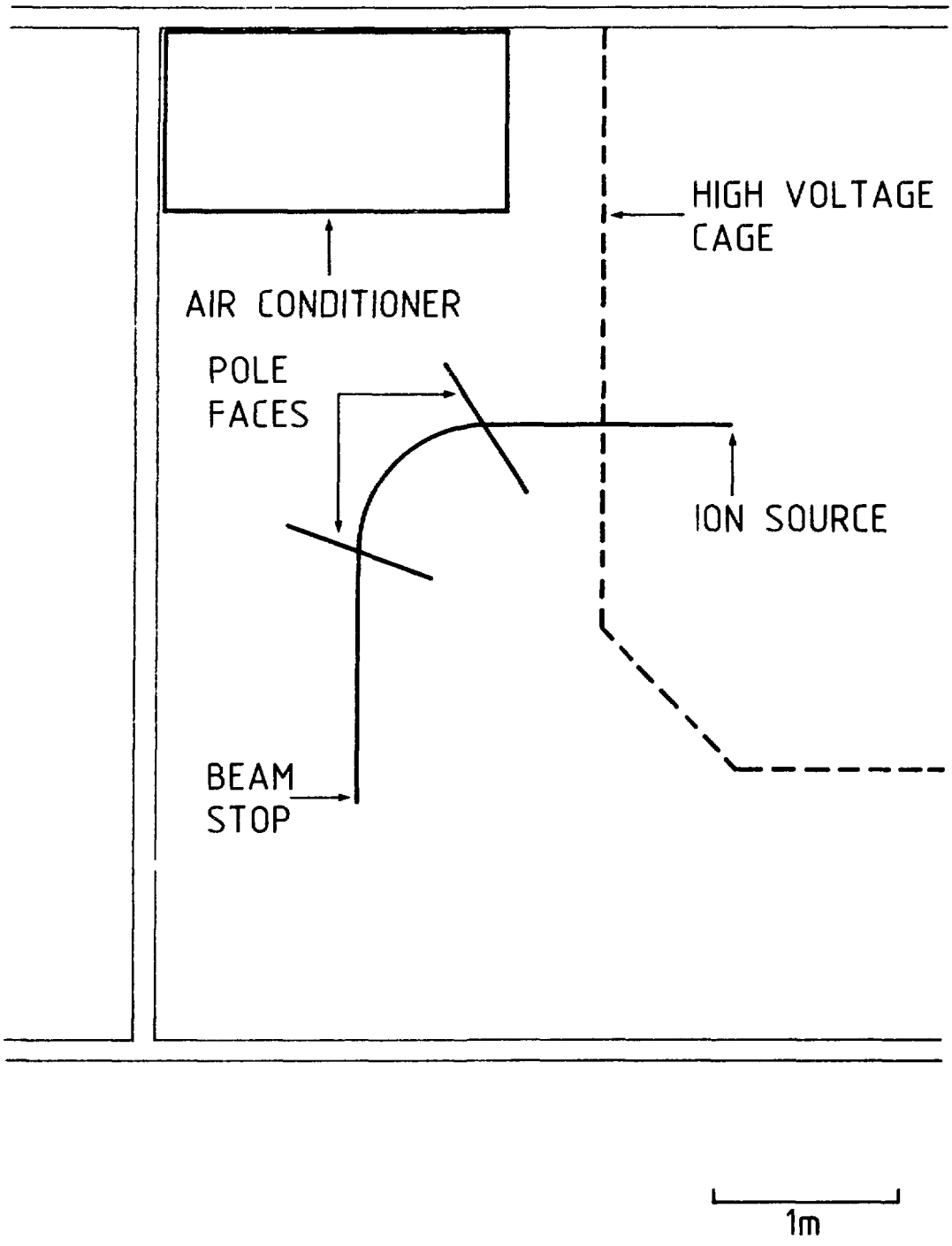

Fig. 1 Layout of separator system in ITE facility.

3.3 Ray Tracing and Beam Envelopes

Detailed beam envelopes were generated for various ions by tracing dozens of individual rays using TRANSOPTR. These provided essential data for the magnetostatics calculations that followed. Specifically, the maximum radial extent of the beam was found to be 143 mm for calcium, the worst case.

The calculations also revealed details of the images that would not otherwise have been obvious. (See Figs. 2-4.) In particular, the images are curved. This aberration could be eliminated by, for example, indexing the magnetic field. The added complication is hardly justified when simply radiusing the image slit can achieve the desired result.

Finally, TRANSOPTR was used to calculate the consequences of inhomogeneities in the magnetic induction. A radially inhomogeneous magnetic induction can be represented by

$$B = B_o\{1-\alpha(R-R_o)/R_o+\beta(R-R_o)^2/R_o^2-....\} \qquad [4]$$

where B_o is the nominal magnetic induction at the mean bending radius, R_o, and B is the magnetic induction at an arbitrary bending radius, R. The coefficients α and β are independent. The former moves the beam waist along the beam axis while the latter influences the radial aberrations. The code can model only the linear radial variations of the magnetic induction. Calculations reveal that an α of 0.05 will move the waist almost 300 mm.

4. MAGNETOSTATICS

4.1 First Approximation

The magnetic rigidity of an ion with kinetic energy E, mass M and charge Z is given non-relativistically by

$$B_oR_o = (300Z)^{-1}(2EM)^{1/2}\ T\cdot m\cdot MeV^{-1}. \qquad [5]$$

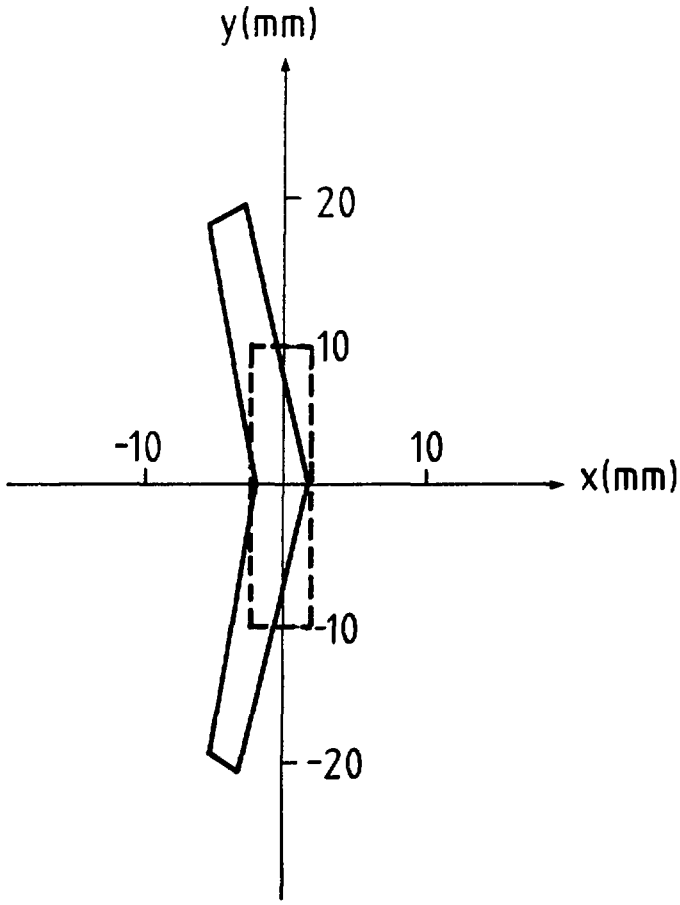

Fig. 2 Beam profile at object (----) and image (——).

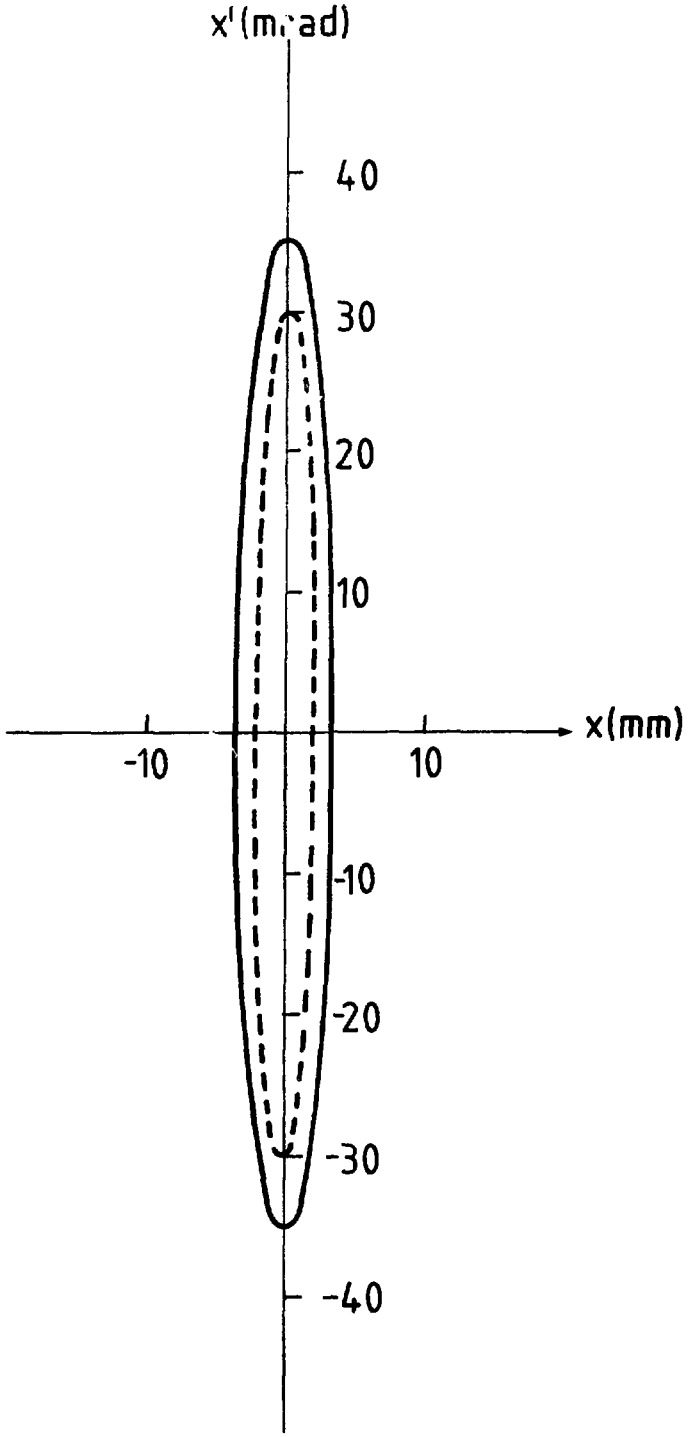

Fig. 3 Radial emittance diagram at object (-----) and image (_____).

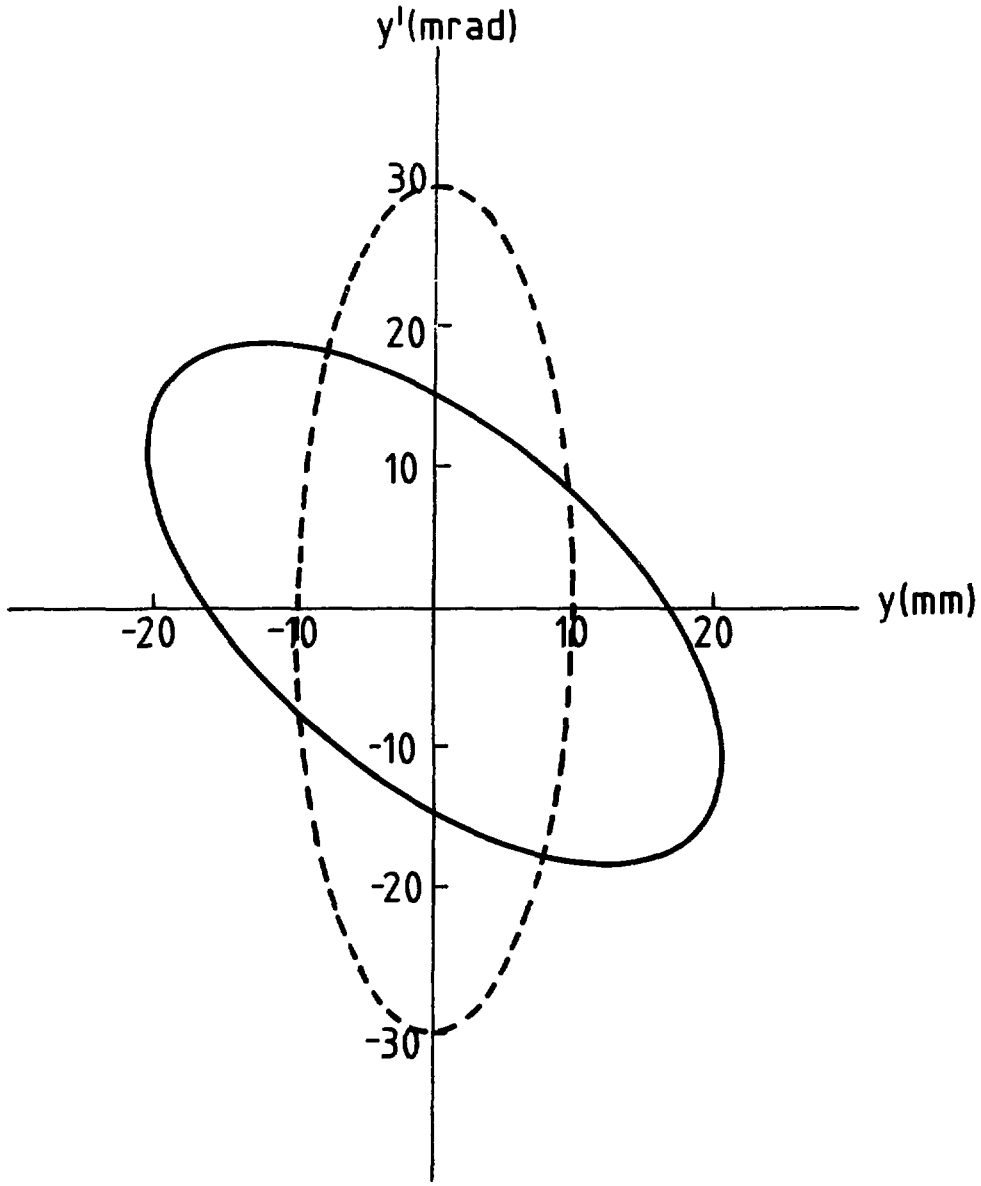

Fig. 4 Axial emittance diagram at object (----) and image (——).

Thus, a magnetic induction of 0.75 T is required to bend a 50 keV singly charged thallium ion at a 620 mm radius. The coil requirements can be deduced from

$$B_o g = \mu_o N i \qquad [6]$$

where g is the pole gap, μ_o is the permeability of free space ($4\pi \cdot 10^{-7}$ T•m/A/turn), N is the number of turns and i is the current. Allowing a 10% margin for leakage and the small, though finite, reluctance of the poles and yoke, 78 000 A•turns are necessary to generate a magnetic induction of 0.75 T across a 120 mm gap. If the current density in the coils is limited to 2.0 A/mm^2, two coils approximately 140 mm by 140 mm will suffice.

The requisite pole width is dictated by the maximum tolerable reduction of magnetic field at the beam edges. If the field reduction is to contribute no more than 10% to the image width, the TRANSOPTR calculations imply that the induction must deviate from the nominal by no more than 0.02%. Tentatively assuming the fringe field distribution deduced by Enge[9], the poles must then extend 156 mm beyond the edges of the beam for a total pole width of almost 460 mm. Again applying Enge's formula, the effective pole edges are calculated to be another 75 mm beyond the hard edges. The corresponding effective pole area is 0.55 m^2. The total cross-sectional area of the return yoke should be at least 0.30 m^2 to limit the magnetic induction to 1.5 T including a 10% leeway for leakage. An H-yoke design that satisfies this criterion and provides for a 10 mm clearance on all sides of the coils is shown in Fig. 5.

4.2 Computerized Optimization

The POISSON group of computer codes[10] was used to model the magnetic circuit. The geometry developed in the previous sub-section was closely approximated in cylindrical coordinates by a 36.7° wedge with the nominal trajectory at a radius of 1.39 m. The permeability of AISI 1020 steel was assumed for both the poles and the yokes. The calculations revealed first that the field uniformity was still adequate even if the pole width was reduced by 20 mm, second that the coils need to supply only 72 000 A•turns rather than the 78 000 A•turns calculated earlier and third that the magnetic induction was in excess of 1.5 T at

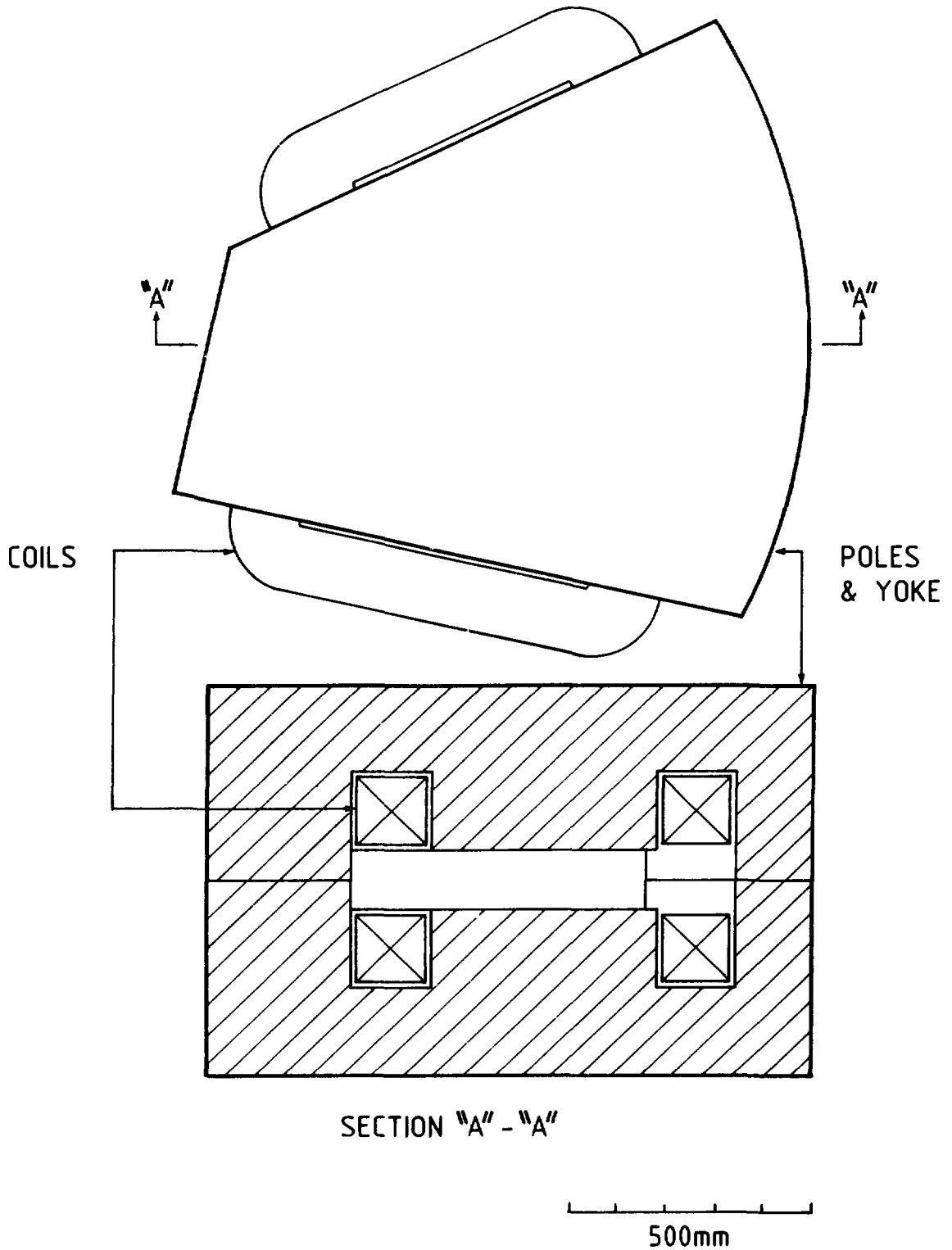

Fig. 5 Configuration of poles, yokes and coils.

the inside corners of the yokes. Reducing the pole width reduced the yoke fields to an acceptable level. The coil dimensions were left unchanged giving a slightly more conservative current density.

4.3 Fringing Fields

The computer codes were also used to calculate the fringing fields at the entrance and the exit edges of the magnet. The calculated fringing fields were, in turn, used to deduce an improved first order field profile coefficient of 0.36 from[7]

$$k_1 = \int_{-\infty}^{\infty} (B-B_o)B/(gB_o^2)ds \qquad [7]$$

where s is the position along the particle trajectory through the fringing field. Once the pole width had been established, the radii of the metal edges R_m' and R_m'' that correspond to the desired effective pole face radii R' and R" could be calculated from[9]

$$R^{-1} = (R_m+0.8g)^{-1}+0.7g/w^2 \qquad [8]$$

where w is the pole width. The required radii turned out to be so large that they were set equal to infinity giving effective radii of 2.3 m. The ray tracing calculations were then repeated with the revised field profile coefficient and the adjusted pole face radii. The results were largely unchanged except that the axial focusing was increased slightly.

5. ELECTROMECHANICAL DESIGN

5.1 Poles and Yokes

The poles and the yoke of the magnet are assembled from two mirror image pieces each consisting of a pole and a half yoke. Thus, the gap and the cavities for the coils are machined out of two solid ingots leaving the poles and the yoke

behind. The two pieces with a total weight of 5200 kg are subsequently located with respect to each other by dowels and fastened together by bolts. This design reduces the number of surfaces that have to be machined precisely, minimizes tolerance buildup and facilitates assembly. Three reference holes on the top face of the upper half of the yoke facilitate alignment of the entrance and exit beam lines.

TRANSOPTR and the POISSON group of computer codes were used to deduce the consequences of various hypothetical machining errors. The behaviour of the magnet was particularly sensitive to the deviation of the pole faces from parallelism. Even a misalignment as small as 1 minute of arc displaces the waist 8 mm along the beam axis.

POISSON was also used to calculate the forces on the magnet components. The net load on each half of the magnet is 27 000 kg, well within the yield strength of the steel.

5.2 Main Coils

The two main coils are wound from 51 mm by 1.6 mm copper tape with 0.2 mm thick nomex insulation between turns. Each coil consists of two 75 turn pancakes, one wound clockwise and the other wound counterclockwise. The two pancakes are each wrapped in two layers of 0.2 mm thick fiberglass tape and sandwiched between three copper plates with 6.4 mm copper cooling tubes brazed into grooves milled into the plates. The pancakes are linked electrically and the entire assembly is wrapped in fiberglass tape and vacuum impregnated with epoxy. The coils, each of which weighs 400 kg, are shown in cross-section in Fig. 6. This system is relatively inexpensive to construct, has proven reliable elsewhere[11] and is easily connected to electrical and cooling water supplies.

A current of 240 A is required to produce the necessary 72 000 A•turns. The hot resistance of the two coils when connected in series is estimated to be 0.24 Ω. Thus, the power supply must generate approximately 60 V. The current must be stable to at least one hundred parts per million if the power supply is to contribute no more than one tenth of the peak width.

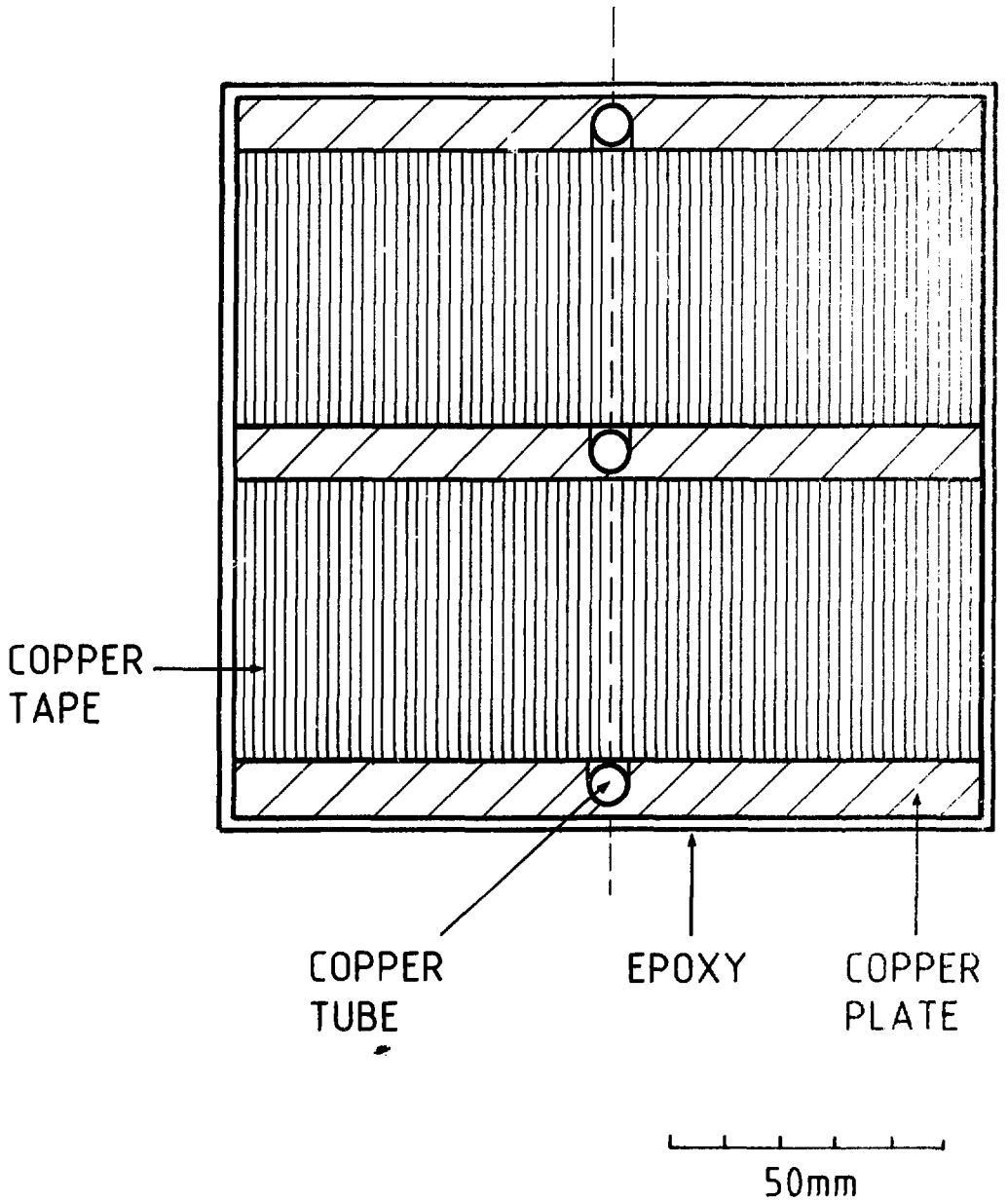

Fig. 6 Typical cross-section of coil.

If the temperature of the cooling water is allowed to rise 10°C between the inlet and the outlet, a flow of 20 L/min will suffice. The pressure drop, with all six cooling channels connected in series, will total about 250 kPa. Assuming that all of the temperature rise occurs across the epoxy saturated fiberglass with a thermal conductivity of 0.2 W/m/°C and a packing factor of 50%, the operating temperature of the coils, given an inlet temperature is 20°C and a film drop of 5°C, will be less than 50°C.

The magnetostatic forces acting on the coils were calculated using POISSON. An axial load of 1600 kg forces the coils against the top and the bottom yoke. The coils are forced against the inside radius of the poles by a radial load of 130 kg. These forces are absorbed by neoprene packing. Stainless steel brackets bolted to the return yokes support the coils when they are de-energized.

5.3 Correction Coils

The rotation of a pole face is equivalent to the introduction of a quadrupole lens. It adjusts the position of the beam waist along the beam axis. A pole face radius has the same effect as a sextupole lens. It influences aberrations. Shims are usually required to optimize the inclination and the curvature of each pole face. Shimming is tedious and, furthermore, cannot take into account the variation of the aberrations with magnetic induction, B_o. Pole face correction coils are easier to implement and to adjust than shims[12].

Correction coils are readily constructed from commercially available circuit boards electrically insulated with kapton film. A quadrupole correction coil is machined into one face and a sextupole correction coil into the other. The coils were designed using[12]

$$\delta\alpha = 4\mu_o R_o Ni/(wgB_o) \qquad [9]$$

where $\delta\alpha$ is the variation in the quadrupolar coefficient, α, and w is the pole width and

$$\delta\beta = 4\mu_o R_o^2 Ni/(w^2 gB_o) \qquad [10]$$

where $\delta\beta$ is the variation in the sextupolar coefficient, β. The conductors for the α-coils are of uniform width. However, the conductors for the β-coils are of various widths given by

$$w_{n-1}^2 - w_{n-1}(w-2w_n) + w_n w = 0 \qquad [11]$$

where w_n is the width of the nth conductor. (Note that the corresponding equation in Ref. 12 is incorrect.) In the present case, assuming twenty-two conductors for each of the top and the bottom coils, the α-coil conductors are 20 mm wide and the β-coil conductors vary from 42 mm at the nominal radius to 11 mm at the extreme radii. The maximum possible correction that can be obtained is limited by the maximum acceptable current density. Based on experience elsewhere[12], circuit board with 0.14 mm thick (4 ounce) conductor should be able to carry as much as 20 A/mm^2. Then $\delta\alpha$ is limited to 0.048 and $\delta\beta$ to 0.068. Similar values have proven to be sufficient on other isotope separators[12].

5.4 Vacuum Chamber

The stainless steel vacuum chamber is equipped with a copper liner that is relatively easily removed for servicing and cleaning. (It is imperative that the liner be cleaned periodically, not only to reduce contamination, but also to minimize the buildup of an insulating layer that could accumulate a static charge adversely affecting the focusing of the beam.) A cross-section of the vacuum chamber with the liner in place is shown in Fig. 7.

The vacuum chamber is a partial annulus with side walls of 9.5 mm thick rolled plate and roof and floor of 7.9 mm thick flat plate. Although the chamber is supported only at the entrance and the exit, the deflection at the midpoint attributable to the approximately 100 kg combined weight of the chamber and the liner is insignificant. On the other hand, the deflection of the roof and the floor due to atmospheric pressure when the chamber is under vacuum is 0.3 mm.

The liner is comprised of two nested pieces, a short straight section that can be withdrawn from the entrance and a long partial annulus that can be rotated

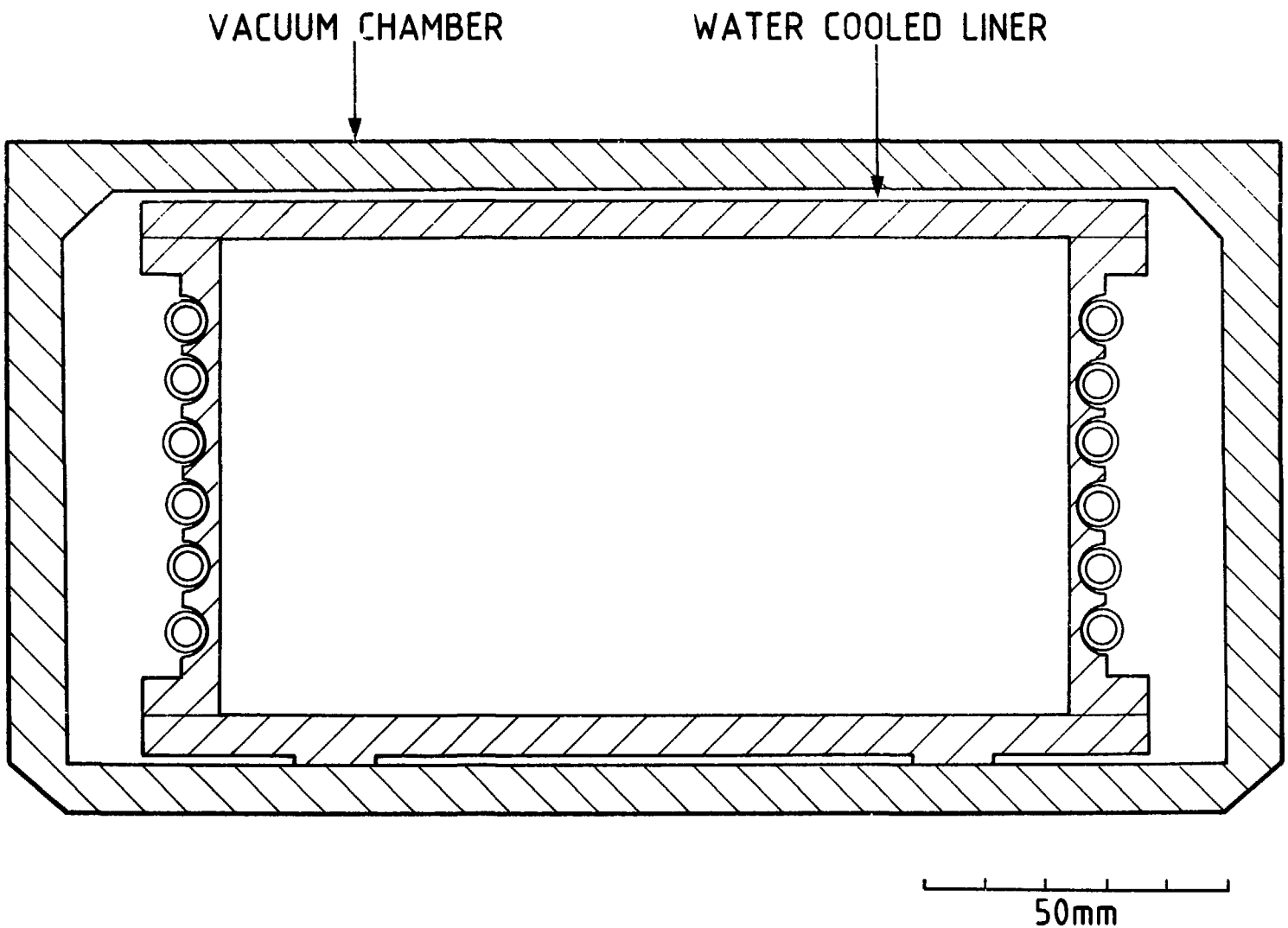

Fig. 7 Typical cross-section of vacuum chamber with water cooled liner.

azimuthally out of the exit. The 6.4 mm thick side walls, with a maximum thermal flux of 3.1 W/mm^2, are water cooled by six 4.8 mm tubes brazed into milled grooves and connected in parallel. If the velocity of the cooling water is limited to 3.0 m/s, the flow will be approximately 20 L/s with an inlet-to-outlet temperature rise of less than 20°C. Then the temperature of the walls should not exceed 50°C. The roof and the floor, with a thickness of 6.4 mm, are subjected to a maximum thermal flux of only 0.04 W/mm . They are cooled mainly by conduction to the side walls to which they are bolted. Their temperature may approach 100°C near the entrance at the nominal bending radius. Each piece of the liner has a flange at one end allowing the cooling tubes to be taken out of the vacuum system for connection to the water supply. The flange on the long section of the liner is positioned with respect to the body of the liner by shimmed brackets so as to ensure that the liner flange seals against the vacuum chamber flange while the liner is supported over its entire length by the vacuum chamber. Although extreme care is necessary in handling the individual pieces of the long liner, the assembly is strong enough to support its own weight of about 40 kg without permanent deformation.

6. CONCLUSIONS

A small simple isotope separation magnet has been designed for the Injector Test Experiment at the Chalk River Nuclear Laboratories. On the basis of suppliers' quotations, the complete system including the poles, the yoke and the coils, the vacuum chamber, the stand and the power supplies should cost no more than 125 000 Canadian 1987 dollars. The details of the design are recorded as CRNL drawings numbered 4522-68 to 4522-80.

7. ACKNOWLEDGMENTS

The authors are indebted to M.S. de Jong, J.H. Ormrod and A.J. Otter for many useful suggestions.

REFERENCES

1. T. Taylor, in "Materials Modification by High-Fluence Ion Beams", ed., R. Kelly, NATO ASI Series, 1987.

2. M.R. Shubaly and M.S. de Jong, IEEE Trans. Nucl. Sci., NS-30 (1983) 1399.

3. A.J.T. Holmes, Phys. Rev. A 19 (1979) 389.

4. V.M. Nezlin, Plasma Phys. 10 (1968) 337.

5. J. Camplan, Nucl. Instr. and Meth. 187 (1981) 157.

6. J.J. Livingood, "The Optics of Dipole Magnets", Academic Press, New York, 1969.

7. E.A. Heighway and M.S. de Jong, Atomic Energy of Canada Limited, Report AECL-6975 (Rev. A), 1984.

8. K.L. Brown, Stanford Linear Accelerator Centre, Report SLAC-75, 1967.

9. H.A. Enge, Rev. Sci. Instr. 35 (1964) 278 and in "Focusing of Charge Particles", ed., A. Septier, Academic Press, New York, 1967.

10. M.T. Menzel and H.K. Stokes, Los Alamos National Laboratory, Report LA-UR-87-115, 1987 and J. Warren et al., Los Alamos National Laboratory, Report LA-UR-87-126, 1987.

11. H.F. Glavish, private communication.

12. J. Camplan and R. Meunier, Nucl. Instr. and Meth. 186 (1981) 445.

ISSN 0067 - 0367

To identify individual documents in the series we have assigned an AECL- number to each.

Please refer to the AECL- number when requesting additional copies of this document

from

Scientific Document Distribution Office
Atomic Energy of Canada Limited
Chalk River, Ontario, Canada
K0J 1J0

Price: A

ISSN 0067 0367

Pour identifier les rapports individuels faisant partie de cette serie nous avons assigné un numero AECL à chacun.

Veuillez faire mention du numéro AECL- si vous demandez d'autres exemplaires de ce rapport

au

Service de Distribution des Documents Officiels
L'Energie Atomique du Canada Limitee
Chalk River, Ontario, Canada
K0J 1J0

Prix: A

971 88